CrossMark

Application and evaluation of ground surface pre-grouting reinforcement for 800-m-deep underground opening through large fault zones

Deyu Qian[1] (ID) · Nong Zhang[1] · Mingwei Zhang[2] · Hideki Shimada[3] · Peng Cao[4] ·
Yanlong Chen[2] · Kai Wen[3] · Sen Yang[1] · Nianchao Zhang[1]

Abstract Faults are complex geological conditions that are commonly encountered during underground excavation. Many support schemes, such as using a single pilot heading method and 30-m-long borehole pre-grouting, have been implemented during the pilot excavation of an 800-m-deep underground opening that passes through large fault zones in East China. However, various geo-hazards, including groundwater inrush, debris flow, and roof collapse, are still occurring, which seriously threaten tunneling safety. To eliminate the geo-hazards and ensure tunneling safety, ground surface pre-grouting (GSPG) was proposed and implemented for the first time to reinforce the regional engineering rock mass for this proposed 800-m-deep underground opening passing through large fault zones. The minimum grouting pressure of GSPG at a depth of 800 m below the surface is put forward based on hydraulic fracturing theory, providing valuable guidance for GSPG engineering practice. Engineering practice demonstrates that GSPG eliminates geo-hazards, improves the objective rock mass stability, and ensures tunneling safety. Field measurements indicate that the displacement velocity of the surrounding rock shows an obvious fluctuation response under the influence of GSPG, and the impact of GSPG on the stability of the 800-m-deep underground opening that has been excavated dramatically decreases as the distance from the grouting borehole increases. Moreover, there is a strong negative exponential correlation between the maximum velocity of deformations and the distance from the grouting borehole. In addition, the safe distance underground during GSPG is greater than 137 m.

Keywords Fault zones · Underground opening · Geo-hazards · Ground surface pre-grouting · Grouting pressure

Introduction

Faults are complex geological conditions commonly encountered during underground excavation (Liu et al. 2010a; Jeon et al. 2004). Many instability problems related to underground openings during excavation and operation are caused by faults, regardless of whether the fault is exposed or concealed during excavation (Hao and Azzam 2005; Schubert and Riedmüller 1997). Fault-related instability problems and geo-hazards are often serious threats to the safety of tunneling in an underground opening and have an impact on the long-term stability of the opening (Hao and Azzam 2005). A large rock mass volume collapsing into an underground opening is a common issue encountered during excavation in areas through large fault zones (Brekke and Howard 1973; Buergi et al. 1999; Hoek 1999). Another common issue is the slide behavior along fault planes and the collapse of blocks intersected by faults and minor fractures into the opening (Nagelhout and Roest 1997). Other issues that affect excavation and operations in underground openings in large deep

✉ Deyu Qian
  deyuqian@gmail.com

[1] School of Mines, Key Laboratory of Deep Coal Resource Mining, Ministry of Education, China University of Mining and Technology, Xuzhou 221116, China

[2] State Key Laboratory for Geomechanics and Deep Underground Engineering, China University of Mining and Technology, Xuzhou, Jiangsu 221116, China

[3] Department of Earth Resources Engineering, Faculty of Engineering, Kyushu University, Fukuoka 819-0395, Japan

[4] School of Mechanical and Chemical Engineering, The University of Western Australia, 35 Stirling Highway, Perth, WA 6009, Australia

 Springer

fault zones include groundwater inrush, debris flow, frequent excessive groundwater inflow, and excessive deformations caused by swelling fault rocks (Dalgıç 2003; Riedmüller and Schubert 2000).

Because of the potential geo-hazards, such as collapse, groundwater inrush and fault slip, during deep underground excavation through large fault zones, it is difficult to provide adequate support or reinforcement for a fractured rock mass with sufficient speed after excavation. It should therefore be practicable and possible to reinforce the fractured rock mass in advance of excavation. During the pilot excavation of an 800-m-deep underground opening passing through large fault zones in the Guqiao Coal Mine in the Huainan mining area in East China, many underground support schemes, such as using a single-pilot heading method and a 30-m long borehole pre-grouting method, were implemented. However, various geo-hazards still occurred, including groundwater inrush, debris flow, and roof collapse, which seriously threatened tunneling safety. To improve the tunneling safety and stability of the 800-m-deep underground opening passing through large fault zones in the Guqiao Coal Mine, ground surface pre-grouting (GSPG) was proposed and carried out to block water-bearing faults and improve the mechanical performance of the rock mass in the large fault zones. Until now, there have been few studies on GSPG reinforcement for a deep underground opening passing through large fault zones. This study primarily focuses on issues related to GSPG, such as analysis of grouting pressure, examination of the impacts of GSPG on the stability of deep underground openings, and quality assessment of the grouting effect. It is significant to study GSPG reinforcement for deep underground openings passing through large fault zones, especially in underground coal mines in East China, as well as other deep underground excavations in areas with similar complex geological conditions.

Geological profiles

The Guqiao Coal Mine, which has had an annual coal production of over 11 Mt. since 2009, is one of the largest coal mines in the Huainan mining area (Fig. 1); it is an important energy source for the rapid economic growth and industrialization of East China. A combined development system that consists of vertical shafts, two mining levels (one at −780 m and the second at −950 m), and a coal lift with one main shaft is used in the mine. The coal mine is divided into four mining districts: the central district, eastern district, northern district, and southern district. Currently, the central mining district is being exploited, while the others are under construction.

The south rail and haulage underground openings, with a horizontal spacing of 30–40 m at the mining level of −780 m, connect the central mining district to the southern mining district, both of which are key transport channels in the Guqiao Coal Mine. The south underground opening will inevitably

Fig. 1 Huainan and Huaibei large coal industry base, with an annual coal production capacity of over 100 Mt., in China
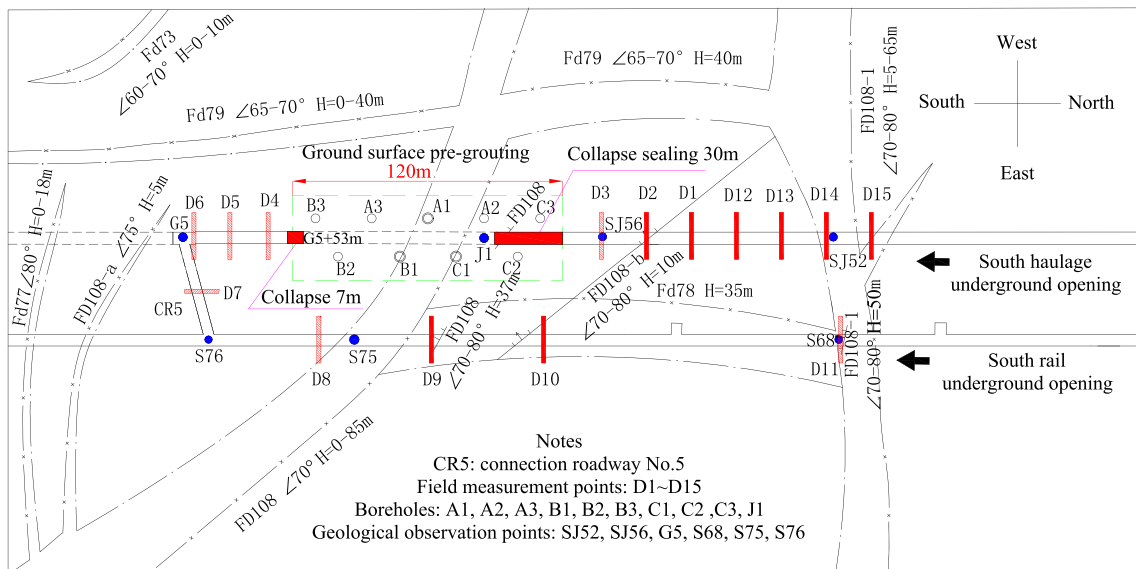
Fig. 2 Plan view of the geological structures, GSPG layout, and field measurement points around the south underground openings. *SJ52* and *S68* are two geological observation points at the interface between geological anomaly fault zones and a normal location in the south haulage and the rail underground opening, respectively

pass through large fault zones, where there are many faults and fractures that are extremely complex, as shown in Figs. 2 and 3. The profiles of the main faults are illustrated in Table 1. The structural form in the section is a large graben composed of eight main step-shaped normal faults with an east–west (EW) direction on the strike and a dip in the south–north direction. The fault group, with a maximum combined throw of 140 m, is 670 m long from north to south.

Based on drill core logs and surface geological boreholes (SGBs), the rock quality designation (RQD) values are generally less than 25%. The RQD is zero within fault fracture zones, which reflects that the rock mass is extremely broken. The pilot underground excavation, which passed through fault FD108-1, also shows small faults and fractures that are well developed, and the surrounding rock is generally broken. The surrounding rock mass is mainly composed of mudstone, sandy mudstone, argillaceous rock, and sandstone in the areas in which the underground openings will pass through. X-ray diffraction (XRD) testing indicates that the rock mass mainly consists of the following: over 78% clay minerals (52.4% kaolinite, 4.6% illite, 3.8% smectite, and 18.1% illite and smectite interstratified mineral) and 13.6% quartz. Therefore, the lithology is mainly composed of argillaceous rock. The rock mass contains closely spaced fractures, which are normally filled with clay fault gouge. Moreover, the groundwater pressures within the large fault zones are high.

Based on the results of in situ stress measurements at 800 m below the surface, the magnitudes of the vertical, maximum
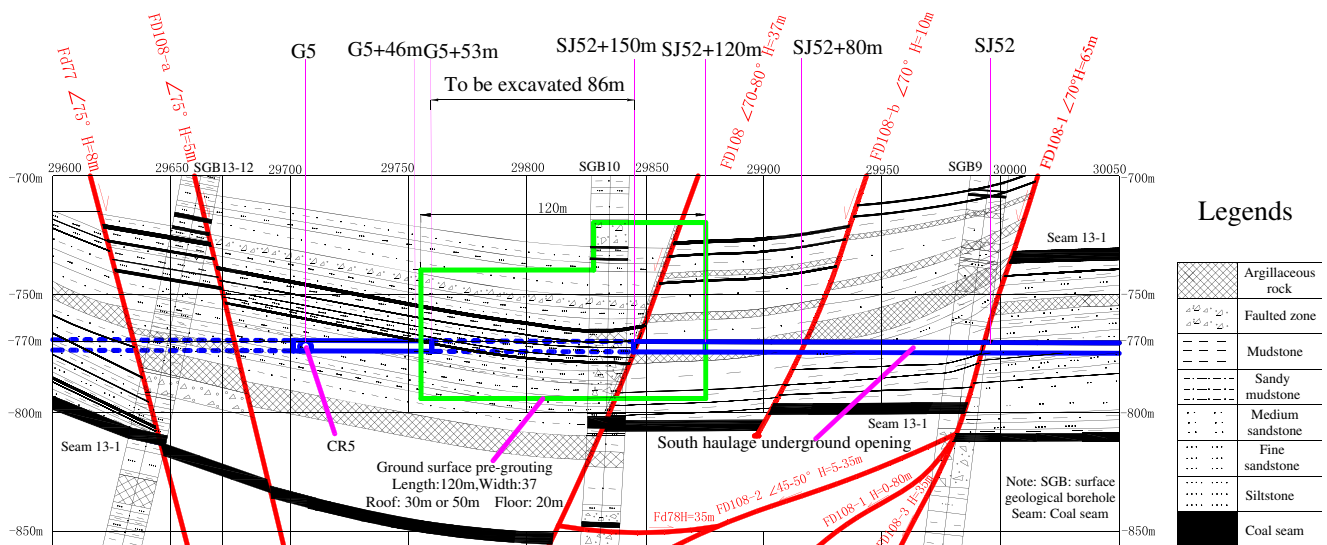
Fig. 3 Section of the geological structures around the south haulage underground opening

Table 1 Profiles of main faults that the deep underground opening passing through

Fault no.	Location	Category	Dip angle	Strike	Throw height (m)	Width of aperture with fillings of fault gouge (m)
FD108-1	SJ52	Normal	70°	EW	65	4.3
FD108-b	SJ52 + 78 m	Normal	70°	NW	10	<4
FD108	SJ52 + 148.8 m	Normal	70–80°	N130°W	37	12
FD108-a	SJ52 + 319 m	Normal	75°	N120°W	5	<4
Fd77	SJ52 + 362 m	Normal	75°	N245°S	0–18	<4
Fd76	SJ52 + 425 m	Normal	80°	N265°S	0–5	<4
F114-a	SJ52 + 493 m	Normal	50–70°	NW	5–15	<4
F114-1	SJ52 + 553 m	Normal	70–80°	NW	0–20	9.3

Fault throw is the relative displacement of opposite fault plane surfaces

principal horizontal and minimum principal horizontal stresses are 18.08 MPa (s), 28.78 MPa (σ_1), and 16.34 MPa (σ_3), respectively. The in situ stress field is dominated by horizontal tectonic stress. The orientation of the maximum horizontal stress is nearly in the EW direction, which is approximately perpendicular to the deep underground opening axis. Given the 16-m-deep test depth in the vertical borehole for in situ stress measurements, the magnitude of the vertical stress (18.08 MPa) is accurate at 816 m below the surface. The average unit weight of the rock is approximately 22 kN/m^3. According to the classification of surrounding rock in the rock roadway for coal mines (Yuan et al. 2011) and the China national standard for the engineering classification of rock mass (GB/T 50218-2014) (Ministry of Water Resources of the People's Republic of China 2015), the surrounding rock of the south underground openings through the fault zones belongs to category V (Qian 2015). The corresponding mechanical parameters of the rock mass can also be obtained according to the surrounding rock classification, as shown in Table 2 (Liu et al. 2010b; Yuan et al. 2011). The uniaxial compressive strength (UCS) of the engineering rock mass is less than 1.6 MPa.

Geo-hazards encountered during the excavation of deep underground openings through large faults

Engineering project profiles

The south underground openings were excavated at a depth of approximately 800 m below the ground surface. The cross-section had a semicircle-arch crown shape with a straight sidewall. The excavation cross-section was 6.0 m in width and 4.6 m in height, whereas the cross-section after the application of U-shaped steel sets and shotcrete support was 5.6 m wide and 4.4 m high. Different methods of excavation and support were proposed and used during the pilot excavation through the large fault zones, such as a single heading method, with a small cross-section of 4.6 m wide and 3.5 m high, and 30-m-long borehole pre-grouting. The strongest support scheme among the different methods of excavation and support adopted was performed when the pilot excavation approached fault FD108 as follows.

Step 1: Five advanced exploration boreholes and six advanced drainage boreholes were created to investigate the geological conditions and conduct gas and groundwater drainage.

Table 2 Physical-mechanical parameters of surrounding rock mass in deep rock roadway

Category	Specific weight γ (kN/m^3)	Friction φ (°)	Cohesion C (MPa)	Tension σ_t (MPa)	Strength R_c (MPa)	Elastic modulus E (GPa)	Poisson's ratio/υ
I	26–27	>60	>2.0	>1.1	>15.0	>25	<0.22
II	25–26	49–60	1.5–2.0	0.9–1.1	8.0–15.0	15–25	0.25
III	24–25	38–49	1.0–1.5	0.5–0.9	4.1–8.0	6–15	0.30
IV	22–24	27–38	0.5–1.0	0.2–0.5	1.6–4.1	2–6	0.325
V	19–22	<27	<0.5	<0.2	<1.6	<2	>0.35

Step 2:   Then, advanced 30-m-long borehole pre-grouting was carried out to reinforce the proposed excavation zone (Fig. 4a, b). The spacing of the adjacent boreholes in the roof was 800 mm. The diameter of the drill bit was 113 mm, and the outer diameter of the steel pipes, with a wall thickness of 8 mm, was 73 mm. The grouting materials were ordinary Portland cement, with a strength grade of 52.5 MPa, and sodium silicate (3–5% by weight). The water-to-cement ratio was 0.8–1.0. The final grouting pressure was generally designed to be 20 MPa and not less than 15 MPa. However, the actual final grouting pressure was between 3 and 22 MPa due to the complex in situ geological conditions. The maximum and minimum cement grouting quantities of the boreholes were 0.8 and 9.8 t, respectively. The total actual grouting quantities of the cement and sodium silicate were 102.7 t and 464 kg, respectively.

Step 3:   Fifteen-meter-long advanced shed-pipe pre-grouting boreholes (Fig. 5a, b) were drilled into the roof by using polycrystalline diamond composite bits with a
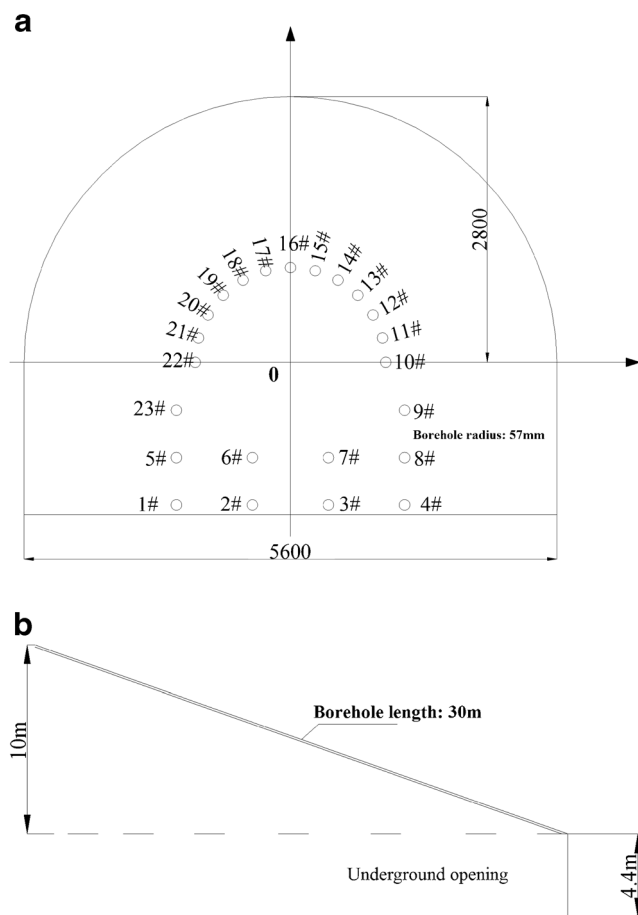
Fig. 4 Layout schematic of 30-m-long advanced borehole pre-grouting. **a** Cross-section perpendicular to the opening axis. **b** Section in the direction of the axis
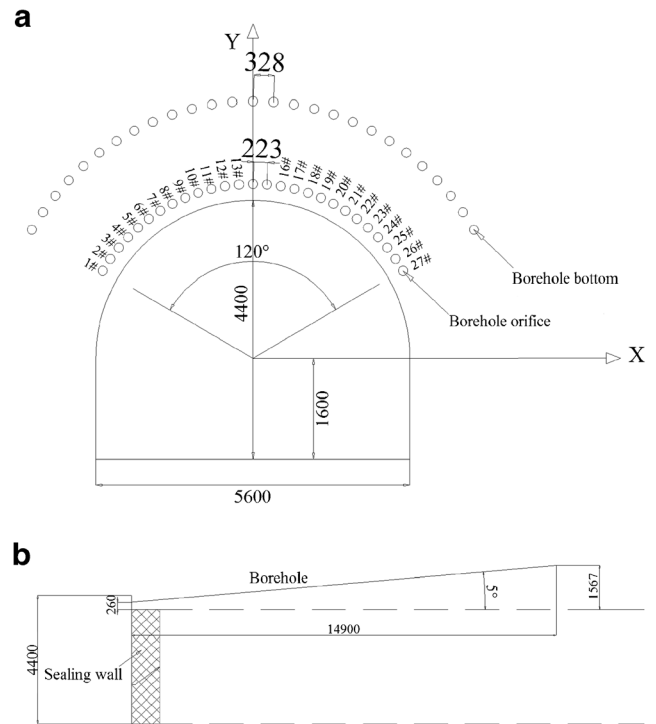
Fig. 5 Layout schematic of 15-m-long advanced shed-pipe pre-grouting support (unit: mm). **a** Cross-section perpendicular to the opening axis. **b** Section in the direction of the axis

diameter of 113 mm. The steel pipe had a core barrel with an outer diameter of 73 mm and a wall thickness of 8 mm. The grouting material was rapid-hardening high-strength sulfoaluminate cement. The designed grouting pressure was 20 MPa. The total actual grouting quantities of the cement and sodium silicate were 52.05 t and 244 kg, respectively.

Step 4:   Five eight-meter-long advanced boreholes pre-grouting with chemical material was performed in the roof at the tunneling face (Fig. 6). The grouting pressure was 8 MPa. The diameter of the drill bit was 42 mm. The spacing of adjacent boreholes was 1400 mm.

Step 5:   U36-shaped steel sets with a spacing of 500 mm were installed after excavation.

Step 6:   After primary shotcrete with a thickness of 70–100 mm was applied, 17 bolts (left-hand twist and IV class thread steel HRB500) and seven cables were subsequently installed to support each cross-section. The shotcrete material was mixed with Portland cement (grade 42.5 MPa), sand, gravel, and water. The proportion of cement, sand and gravel was 1:2:2 by weight. The proportion of water in the shotcrete material was 45%. The accelerating agent-to-cement ratio was 2.5–4%. The diameter and length of the bolts were 22 and 2800 mm,
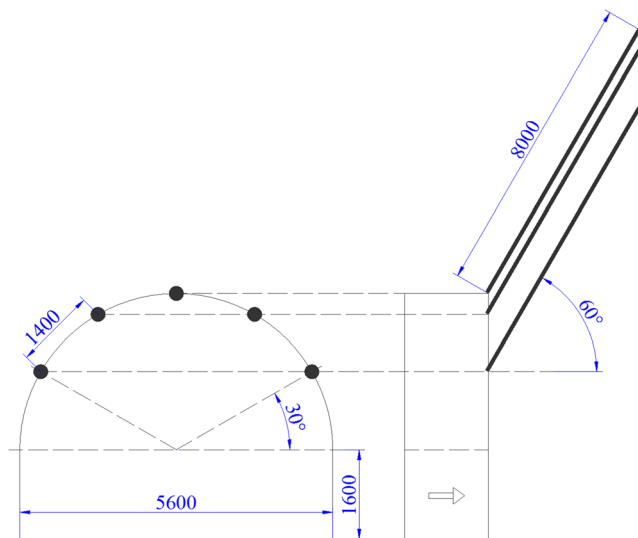
Fig. 6 Layout schematic of 8-m-long advanced borehole pre-grouting (unit: mm)

respectively. The interval and spacing of the bolts were 800 and 1000 mm, respectively. The diameter and length of the cables were 21.8 and 6300 mm, respectively. The spacing between the cables was 1000 mm.

Step 7:   Three-meter-deep holes with Portland cement, with a strength grade of 42.5 MPa, and 8-m-deep holes with superfine cement, with a strength grade of 62.5 MPa, were created after secondary shotcrete with a thickness of 50 mm was applied. The pressures of the 3-m-deep and 8-m-deep holes post-grouting were 2 and 3 MPa, respectively. The water-cement ratio was 0.8–1.0. The spacing of post-grouting holes was 1000 mm.

Geo-hazards encountered during excavation

Different methods of excavation and support were used during the pilot excavation through the large fault zones. However, various geological disasters still occurred during the previous excavation, such as roof collapse, groundwater inrush, and debris flow, which seriously threatened tunneling safety. For example, southern roof collapse occurred as the tunneling face approached the area at G5 + 53 m in the south haulage underground opening even though the pilot heading method had been adopted. Moreover, debris flow and roof collapse occurred in the areas from SJ52 + 120 m to SJ52 + 150 m in the south haulage underground opening when the tunneling face approached fault FD108. The volume of instantaneous debris flow was up to 20 m^3. A sealing wall at SJ52 + 120 m was constructed to block the debris flow and the roof collapse space. The filling materials, composed of cement (grade

42.5 MPa) mixed with 45% water by weight, were pumped to fill the pores in the roof collapse space via the pipes through the sealing wall. Approximately 88.75 t of cement was used to infill the roof collapse space. Then, 30-m-long borehole pre-grouting was carried out; however, the geo-hazards of debris flow and roof collapse occurred once more when the tunneling face approached fault FD108. Afterward, the strongest support scheme among the different methods of excavation and support was performed. However, northern roof collapse and debris flow occurred yet again. The roof collapse in the deep underground opening is shown in Figs. 7 and 8.

Moreover, during the pilot excavation, excessive groundwater inflow, which is frequently associated with faults and fractures, often occurred, including groundwater inrush inflow with a flow rate of 10 m^3/h or higher occurring over 15 times. The maximum water inflow rate was up to 60 m^3/h. The normal groundwater inflow of the complete excavation was 5 m^3/h. The excessive groundwater inflow not only threatened tunneling safety but also further weakened the rock mass over time and decreased the stability of deep underground openings because the argillaceous rock, which contains substantial amounts of clay minerals, undergoes softening, disintegration and swelling when in contact with water. Moreover, the sticking, blocking, and jamming of drill bits and the collapse of boreholes frequently occurred during drilling advanced exploration and the pre-grouting of boreholes at the tunneling face as result of fractured argillaceous rock.

To eliminate geo-hazards, GSPG is proposed to block water-bearing faults and improve the mechanical properties of the regional rock mass in large fault zones. Moreover, GSPG can effectively eliminate the blocking of drill bits and the collapse of boreholes in a fractured rock mass by utilizing mud gravity pressure, casing pipes for borehole wall protection, and the downward grouting method.

Fig. 7 The roof collapse and debris flow at the tunneling face near fault FD108

Fig. 8 The collapsed section of the south haulage underground opening
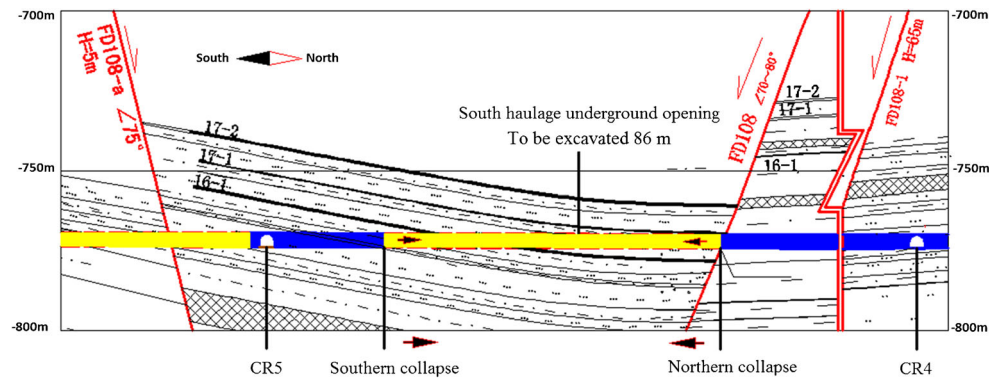
Analysis of GSPG

Mechanism of GSPG

GSPG usually involves the injection of Portland cement with sodium silicate or clay-cement grouting materials into faults, fractures, or dissolution cavities within water-bearing strata. The purposes of grouting are to block water-bearing conduits (faults and fractures), decrease the permeability of the strata, control groundwater inflow, improve the regional engineering rock mass stability in advance, and ensure safety during the excavation and operation of underground openings (Saito et al. 2014; Yang and Wang 2005). The mechanism underlying GSPG's action is the filling of faults and the reinforcing of fractured strata. The grouting slurry, which can squeeze or replace fault gouges and free water within the target strata and change the structure and mechanical properties of the original strata, is directly injected into the formation of faults, fractures, and aquifers. Thus, GSPG can compress the original strata in the region, improve the bearing capacity, and decrease compression deformations of the rock mass through the reduction of pore water pressure after excavation. The slurry diffusion models include filling grouting, compaction grouting, permeation grouting, and hydro-fracture grouting.

Principles of GSPG scope and borehole layout

GSPG scope

The reinforcement scope of GSPG is comprehensively determined based on the hydrogeological and engineering geological conditions and the tunnel construction method. Generally, the grouting reinforcement scope is 2–3 times the excavation radius of underground openings. However, the reinforcement scope should be 4–6 times or more as large as the excavation radius when the groundwater pressure is high or construction is performed under complex geological conditions (Lai et al. 2008).

Borehole layout and height of grouting sub-segment

Depending on the slurry diffusion range of a single borehole, the grouting diffusion of adjacent boreholes should overlap and form a fairly complete grouted rock mass with the necessary thickness in the target area. Grouting sequences are usually carried out from the outside boreholes to the inside boreholes. Grouting for each single borehole is conducted using the multiple sub-segments approach. The appropriate height of each sub-segment is approximately 10 m in extremely broken strata, 15–25 m in broken strata, 25–35 m in intact strata, and 35–80 m for re-grouting (Yang and Wang 2005).

Grouting pressure of GSPG

The grouting pressure is a driving force for overcoming resistance to the flow of the slurry, and it is the energy for filling diffusion, penetration, compaction, and hydro-fracture grouting of slurry injected into the fractured strata. It is closely related to the lithology, aperture and connectivity of fractures, slurry concentration and type, and injection time. A higher grouting pressure leads to greater diffusion, while a low pressure causes insufficient diffusion and negatively affects the effectiveness of water blocking. The grouting pressure is an important indicator of grouting quality.

The particle size of cement slurry is relatively large compared with that of argillaceous rock. Thus, the permeation grouting range is usually small. The diffusion model mainly involves hydro-fracture grouting with the compaction effect. Therefore, the grouting pressure of the bare segments of a circular borehole can be calculated by using hydraulic fracturing theory. The calculation of stresses around a vertically drilled circular borehole can be simplified as a plane strain problem (Fig. 9). According to the solutions for the stress distribution around a circular opening in a medium subjected
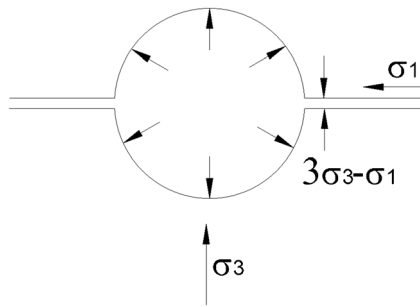
Fig. 9 Schematic of single-borehole hydraulic fracturing

to biaxial stress, the stresses at the borehole boundary are given by the following expressions (Brady and Brown 2004):

$$\sigma_{\theta\theta} = \sigma_1 + \sigma_3 - 2(\sigma_1 - \sigma_3)\cos 2\theta \tag{1}$$

$$\sigma_{rr} = 0 \tag{2}$$

where $\sigma_{\theta\theta}$ is the tangential stress, σ_{rr} denotes the radial stress, σ_1 is the maximum principal horizontal stress, σ_3 represents the minimum principal horizontal stress, and θ is the angle between one point at the borehole periphery and the maximum principal horizontal stress axis.

When $\theta = 0$, the minimum tangential stress $\sigma_{\theta\theta}$ is as follows:

$$\sigma_{\theta\theta\min} = 3\sigma_3 - \sigma_1 \tag{3}$$

According to the principles of the hydraulic fracturing technique (Brady and Brown 2004; Huang et al. 2005), when the grouting pressure P_i exceeds the tensile strength of the rock mass σ_t and the minimum tangential stress, the borehole wall begins to fracture at the periphery ($\theta = 0°$) in the direction of the maximum principal horizontal stress axis. The grouting slurry begins to flow into the strata. As the grouting proceeds, the crack will further expand. The horizontal stress perpendicular to the crack direction in the plane is close to the original rock stress state at a location far from the borehole, where the grouting pressure equals σ_3.

The minimum grouting pressure acting on the strata P_i can be given as follows:

$$P_i = P_1 + P_2 = 3\sigma_3 - \sigma_1 + \sigma_t \tag{4}$$

Therefore, the grouting pump pressure P_1 can be given as follows:

$$P_1 = 3\sigma_3 - \sigma_1 + \sigma_t - P_2 \tag{5}$$

where P_1 is the grouting pump pressure. According to in situ stress measurements in the 800-m-deep underground opening in the Guqiao Coal Mine, σ_1 and σ_3 are 28.78 and 16.34 MPa, respectively; σ_t is the tensile strength of the rock mass, taken

to be 0.15 MPa; and P_2 is the pressure of the grouting slurry, with $P_2 = \gamma h$. h is the designed grouting depth of the bare segments of boreholes, taken to be 750.5–824 m. The water-to-cement ratio is mainly 0.6:1. The bulk density of the grouting slurry (γ) is approximately 17.15 kN/m³. P_2 is between 12.87 and 14.13 MPa.

Substituting the parameters above into Eqs. (4) and (5), the grouting pressure P_i at a depth of approximately 800 m and the grouting pump pressure P_1 can be obtained as follows:

$$P_i = 20.39\text{MPa}, P_i = 6.26\text{–}7.52\text{MPa}$$

Therefore, the minimum grouting pressure is approximately 2.5 times the hydrostatic pressure at a depth of 800 m. The minimum final pump pressure should be greater than 6 MPa when GSPG is conducted at a depth of approximately 800 m. In addition, the minimum grouting pressure is greater than the minimum principal stress σ_3, which could maintain the crack opening and ensure that the grouting slurry flows along the crack direction.

Estimation of the grouting amount and diffusion radius of a single borehole

Grouting amount for a single borehole

The estimation of an accurate grouting amount is difficult before GSPG. To initially estimate the grouting amount, the grouting amount calculation for a single borehole can be simplified as a cylinder (Yang and Wang 2005).
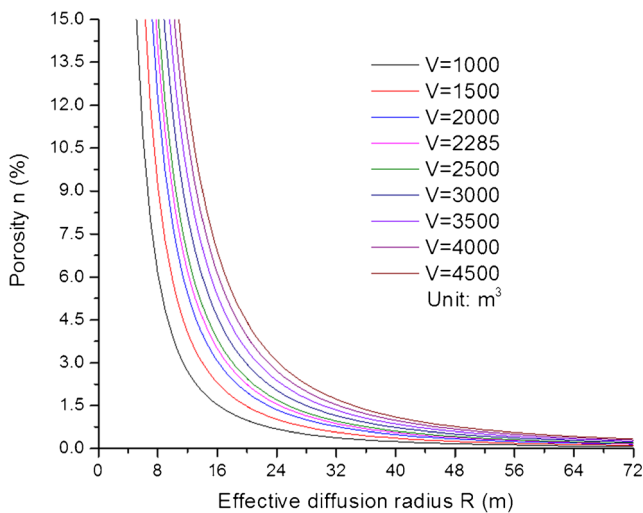
$$V = A\pi R^2 Hn\beta \tag{6}$$

where V is the volume of the grouting amount for each segment of completion for one borehole; A denotes a parameter of grouting wastage, which generally varies from 1.2 to 1.5 (the volume of grouting slurry wasted in blenders, pumps, and pipes during grouting); R is the effective diffusion radius of the grouting slurry of a single borehole; H is the height of the grouting segment; n is the porosity of the fractured rock mass, usually 2.5–6%; and β represents a parameter of fracture filling, generally varying from 0.7 to 1.0 (referring to the extent to which grouting slurry can fill fractures) (Yang and Wang 2005).

Grouting diffusion radius

The effective diffusion radius of grouting slurry is the length to which grouting can effectively block water inflow and improve the performance of the rock mass. Grouting slurry randomly penetrates fractures in terms of direction and distance. Therefore, it is difficult to accurately determine the diffusion

Fig. 10 Correlation of effective diffusion radius of grouting slurry and the porosity

Table 3 Selection of initial water-to-cement ratio

Q (L/min)	60–80	80–150	150–200	>200
Water-to-cement ratio	2:1	1.5:1	1.25 or 1:1	0.8 or 0.6

shift and adjust the grouting parameters in a timely manner, including the grouting pressure, grouting amount, water-to-cement ratio, and grouting sequences, based on the water pressure test and real-time monitoring data during GSPG. For example, the grouting water-to-cement ratio can be appropriately adjusted according to the maximum quantity (Q) of water absorbed by boreholes during the water pressure test, as shown in Table 3 (Yang and Wang 2005).

radius. The radius of grouting slurry diffusion is positively related to the grouting pressure, grouting time, and width of fractures and negatively related to the particle size and viscosity of grouting slurry materials. According to Eq. (5), the relationship curve for the grouting diffusion radius and the porosity is shown in Fig. 10, where we assume that $A = 1.3$, $H = 73.5$ m, and $\beta=0.85$ based on the field data. Obviously, the effective diffusion radius of grouting slurry increases when the porosity decreases, with the assumption that the grouting amount is constant. For example, when $n = 3.5\%$ and $V = 2285$ m^3, the effective diffusion radius of the grouting slurry of a single borehole is 16 m.

Process control principles of GSPG

Process control principles with 4S (stop, slow, switch, and shift) criteria for GSPG are proposed to control the grouting diffusion distance and improve the grouting effect. (a) Stop: Stop grouting to wait for the solidification of the grouting slurry and prevent excessive slurry diffusion within large fault fracture zones if underground grouting leakage occurs or the grouting pump pressure is always zero during GSPG. Intermittent grouting should be used. The internal time should be longer than 36 h. Then, re-grouting is conducted. (b) Slow: Slow the grouting speed and gradually decrease the grouting outflow of the pump if the grouting outflow is still high half an hour after the grouting pressure reaches the designed value. If both the grouting pressure and grouting amount reach the designed values, the sub-segment grouting is completed after the pumping is maintained for half an hour. (c) Switch: Switch to grouting other boreholes when the current borehole grouting is stopped due to grouting leakage or while waiting for solidification of the grouting slurry. (d) Shift: Dynamically

Engineering practice

### Design scheme for GSPG

GSPG scope and borehole layout

(1) Grouting scope and borehole layout
This GSPG project used vertical and S-shape branch boreholes to block water-bearing faults and fractures and to improve the strength and stability of the fractured rock mass between the northern and southern collapse in the large fault zones. In practice, nine GSPG boreholes were drilled along the two sides of the proposed haulage underground opening in the fault core area. The GSPG grouting reinforcement range was approximately 120 m long and 37 m wide. The height for the grouting segment was approximately 73.5 m in the northern area around fault FD108, including boreholes A2, C1, C2, and C3, and 53.5 m in the southern area containing boreholes A1, A3, B1, B2, and B3. The GSPG borehole layout and reinforcement range are shown in Figs. 2, 3, and 11. There are five boreholes with a spacing of 25 m in the west side of the proposed south haulage underground opening, while there are four boreholes with a spacing of 25 or 27.5 m along the east side.

(2) Combination construction of boreholes
The grouting sequences of boreholes are usually conducted from the outside boreholes (e.g., boreholes A2, B2, and C2) to those inside (e.g., boreholes A1, B1, and C1). The boreholes are divided into three groups and drilled by using three separate drilling rigs. Branch boreholes A2, B2, and C2 are drilled in the first round, followed by the drilling of boreholes A3, B3, and C3 in the second round. A1, B1, and C1 are completed in the last round. The application of S-shaped branch boreholes reduces the amount of drilling and hastens construction compared with vertical boreholes.

Fig. 11 Sketch map of GSPG borehole layout
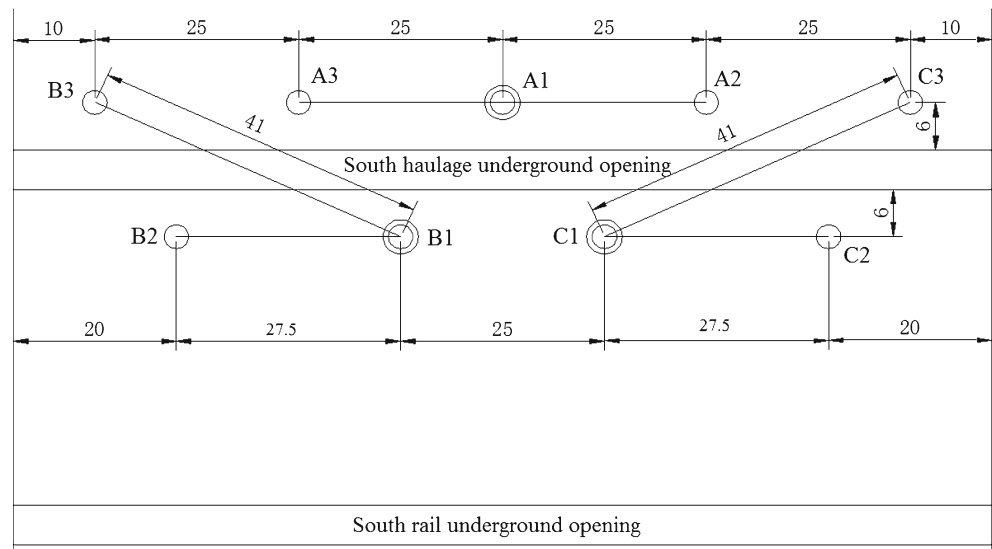
(3)   Borehole structure

The borehole structure is shown in Fig. 12. For 0–500.00 m deep strata (30–40 m below the bedrock surface), the borehole diameter is 244.5 mm, and the specification of casing pipes for borehole wall cementation is a diameter of 194 mm and a wall thickness of 7 mm. The application of casing pipes for borehole wall cementation is carried out to prevent grouting slurry leakage during grouting. For 500.00–750.50 m or 770.50 m deep strata (the top boundary of the grouting segment), the borehole diameter is 165.1 mm; for 650.50 m (or 670.50 m)–750.50 m deep (or 770.50 m) strata (the top boundary of the grouting segment), the specification of casing pipes for borehole wall cementation is a diameter of 146 mm and a wall thickness of 6 mm. The borehole diameter is 118 mm from 750.5 or 770.50 m (the top boundary of the grouting segment) to 824.0 m deep (the bottom border of the grouting segment).

GSPG process

(1)   Division of the grouting sub-segment height

To ensure grouting quality, a short multiple segment approach should be adopted during grouting in heavily fractured rock masses. In practice, the grouting of boreholes is carried out for every 10-m-high sub-segment to eliminate the blocking of drill bits and borehole collapse and to improve the effects of grouting.

(2)   Grouting materials

The grouting material is mainly composed of ordinary Portland cement, sodium chloride, and triethanolamine mixed with water. The strength grade of the cement is 42.5 MPa. The water-to-cement ratio is 0.6:1–1.5:1. In practice, 80% of the total grouting material uses a water-to-cement ratio of 0.6:1 due to the large consumption of grouting material in the large fault zones. Based on the grouting situation, sodium chloride

and triethanolamine could be used as early strength additives, accounting for 5 and 0.5‰ of the total cement consumption by weight percent, respectively.
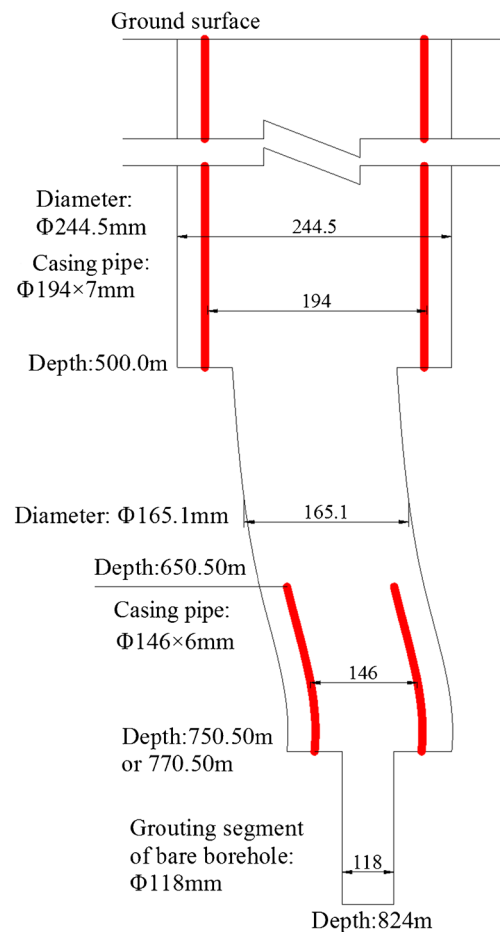

Fig. 12 Sketch of S-shape branch borehole structure

Table 4 Comparison of designed and actual grouting amount

Borehole	Height of grouting segment (m)	Designed grouting amount (m³)	Designed grouting amount per meter (m³/m)	Actual grouting amount (m³)	Actual grouting amount per meter (m³/m)	Actual cement amount (t)	Difference of grouting amount (m³)
A1	53.5	1663.23	31.1	1478	27.6	1353	−185.23
A2	73.5	2285	31.1	2682	36.5	2335.82	397
A3	53.5	1663.23	31.1	1280	23.9	1029.92	−383.23
B1	53.5	1663.23	31.1	978	18.3	757.26	−685.23
B2	53.5	1663.23	31.1	1467	27.4	1453.98	−196.23
B3	53.5	1663.23	31.1	1820	34.0	1455.08	156.77
C1	73.5	2285	31.1	1990	27.1	1633.32	−295
C2	73.5	2285	31.1	4036	54.9	3889.4	1751
C3	73.5	2285	31.1	3322	45.2	3122.22	1037
Total	561.5	17,456.2	/	19,053	/	17,030	1596.8

(3) Grouting amount

According to Eq. (6), the total designed grouting amount for the nine boreholes is obtained as follows:

$$V = A\pi R^2 Hn\beta = 17456.2 \text{ m}^3$$

where V is the total volume of the grouting amount used in all segments for the nine grouting boreholes; A is taken to be 1.3; R is taken to be 16 m; H is the total height of the grouting segments in all nine boreholes, taken to be 561.5 m, as shown in Table 4; n is taken to be 3.5%; and β is taken to be 0.85.

(4) Design grouting pressure

The minimum final grouting pump pressure should exceed 6 MPa.

(5) Workflow process

To control accidental blocking of the drill bit and collapse of the borehole in the fractured rock mass zones and to solve the problem of the installation difficulty of stop-grouting plugs in high dip angle fracture zones, the downward grouting method with short multiple grouting sub-segments (approximately 10 m high) is applied. The GSPG workflow process is illustrated in Fig. 13. The field site of GSPG on the surface is show in Fig. 14.

Fig. 13 Flow chart of the GSPG process
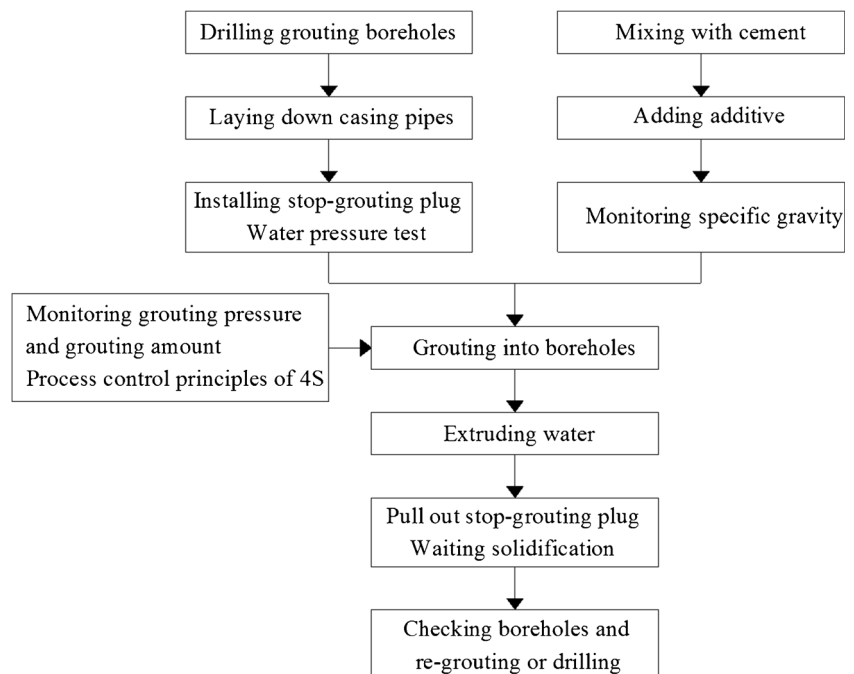
Fig. 14 The field site of GSPG
on the surface

Layout of field measurement points for GSPG

To control the grouting process and analyze the influence of GSPG on the stability of deep underground openings, field measurements, such as surface displacements and grouting leakage, are carried out during GSPG. The measurement points are shown in Fig. 2 and Tables 5 and 6. The layout of the measurement points for monitoring surface displacements is shown in Fig. 15. The monitoring data include distances AB, CD, OA or OB, and OC or OD as time increases. The meaning for the change of the distances is shown in Table 7. Moreover, the monitoring data on the ground surface include the actual pre-grouting amount, grouting pressure, and cement-to-water ratio.

Results and discussion

Actual grouting amount and porosity of the engineering rock mass

The designed and actual grouting amounts are shown in Table 4. The actual grouting amount per meter height is

18.3–54.9 m^3. The grouting amount for boreholes (A1, B1, and C1) in the middle area is less than that for the peripheral boreholes. The grouting amount for boreholes (A2, C1, C2, and C3) around fault FD108 in the northern area is greater than that for boreholes (B1, B2, B3, A1, and A3) in the southern area owing to the influence of large faults. The maximum grouting amount for a single borehole is 4036 m^3 at borehole C2, while the minimum grouting amount is only 978 m^3 at borehole B1.

The total actual grouting amount is 19,053 m^3, which is an increase of 9.1% in comparison with the designed grouting amount of 17,456.2 m^3 because a lower porosity (3.5%) of the engineering rock mass in the northern grouting areas was used for the initial estimation. According to the re-calculation of the actual pre-grouting amount, the porosities in the southern and northern (around fault FD108) target areas for the haulage underground opening are approximately 3.0 and 4.6%, respectively.

Actual grouting pressure

Based on the monitoring data, when the grouting segment depth and grouting amount of different boreholes are identical

Table 5 Field measurement points in deep underground openings during GSPG

No.	D1	D2	D3	D4	D5	D6	D7	D8
Location	SJ52 + 64 m	SJ52 + 84 m	SJ52 + 104 m	SJ52 + 252 m	SJ52 + 269 m	SJ52 + 285 m	S76 + 20 m	SJ68 + 230 m
No.	D9	D10	D11	D12	D13	D14	D15	/
Location	SJ68 + 180 m	SJ68 + 130 m	SJ68	SJ52 + 44 m	SJ52 + 24 m	SJ52 + 4 m	SJ52-16 m	/

Table 6 The horizontal distances of some measurement points relative to boreholes	Measurement points no.	D1	D2	D3	D12	D13	D14	D15	D9	D10
	Distance from borehole A2 (m)	92	72	52	112	132	152	172	58	60
	Distance from borehole C2 (m)	77	57	37	97	117	137	157	52	38
	Distance from borehole B2 (m)	157	137	117	177	197	217	237	56	100

during GSPG, the grouting pump pressures for boreholes A2, C1, C2, and C3 are usually less than those for boreholes B1, B2, B3, A1, and A3 owing to the influence of faults and fractures. The grouting pump pressure for several boreholes is generally low (approximately 0–6 MPa) in the beginning of GSPG. However, the pressure begins to increase as the grouting slurry gradually fills the fractured rock mass. The maximum and minimum final pump pressures among all nine boreholes are 11 and 6 MPa, respectively, as shown in Table 8, which are generally inconsistent with the minimum theoretical value (6 MPa). The corresponding maximum and minimum grouting pressures at the borehole bottom are approximately 25 and 20 MPa, which are 2.5 times larger than the hydrostatic pressure at a depth of 800 m. For example, the grouting pump pressure and grouting amount for borehole C2 are illustrated in Fig. 16. The total grouting amount for 16 occurrences of grouting is 4047 m^3. The final pump pressures of grouting are between 6 and 11 MPa. Therefore, the final pump pressure can meet the GSPG requirement.

Maximum grouting diffusion distance and influence of faults on GSPG

According to the monitoring records, there are nine occurrences of grouting slurry leakage at the beginning of GSPG. Six occurred near fault FD108 in the rail underground opening, while three occurred in the haulage underground opening, with two appearing near fault F108-b. This indicates that faults are the main channels of grouting diffusion and have a large impact on the quality of grouting. Underground grouting slurry leakage monitoring shows that many fault gouges,

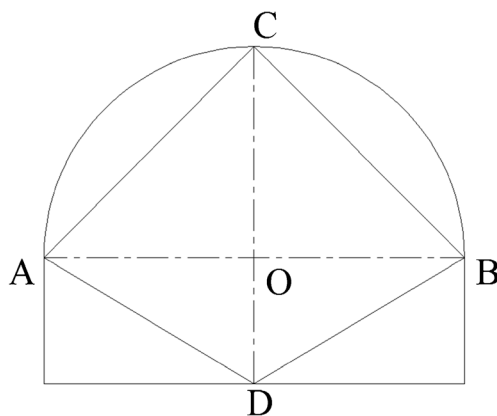Fig. 15 Layout of measurement points for monitoring surface displacements

argillaceous infillings, and coal and broken rock fragments have been squeezed out from the large fault zone by the grouting. Therefore, the grouting cement slurry of GSPG replaces the fault gouges and argillaceous infilling and reinforces the fault fracture zone.

The designed grouting diffusion radius is 16 m. However, according to the grouting leakage record, as shown in Table 9, the maximum actual grouting diffusion distance in the beginning of GSPG is as high as 40–72 m in the plane due to the impact of large faults. The maximum vertical grouting diffusion distance is as high as 22 m. To control excessive diffusion for grouting slurry and grouting leakage, the "4S" grouting process control principles are used during GSPG.

Influence of GSPG on the stability of deep underground opening

The intermittent grouting operation of branch boreholes A2, C2, and B2 is first alternately carried out. The displacements and velocities of the haulage underground opening during GSPG are graphically presented in Figs. 17, 18, and 19.

(1) According to the jump change and fluctuation response of the displacement velocity of the surrounding rock, GSPG significantly disturbs the stability of the deep underground opening. GSPG can further lead to serious deformations for the deep underground openings in the large fault zones due to the influence of shock loads from the intermittent grouting. For instance, the creep rates of sidewall-to-sidewall and roof-to-floor displacement at measurement point D3 before GSPG are 1.94 and 4.12 mm/day, respectively (Fig. 17). However, they are as high as 200 and 445 mm/day, respectively, during GSPG, which are 103 times and 108 times as large as that of the corresponding velocities before GSPG. The influence of GSPG on the stability of deep underground opening excavation is quite dramatic and surprising due to the dynamic load from the grouting slurry pressure.

(2) The impact of GSPG dramatically decreases when the distance from the grouting borehole increases. Moreover, the time when the maximum velocity occurs is obviously delayed with increasing distance. For example, the maximum velocities of sidewall-to-sidewall and roof-to-floor displacements at measurement point D3, which is 37 m from borehole C2, are 200 and 445 mm/day, respectively, on the eighth day after GSPG (Fig. 17).

Table 7   The meaning for the change of the distances monitored

Distance change	AB	OA	OB	CD	OC	OD
Displacement	Sidewall-to-sidewall	Left sidewall	Right sidewall	Roof-to-floor	Roof	Floor

Table 8   The maximum and minimum final grouting pump pressures among all nine boreholes

Boreholes	A1	A2	A3	B1	B2	B3	C1	C2	C3
Minimum final pump pressures (MPa)	8	6	8	8	8	7	6	6	6
Maximum final pump pressures (MPa)	11	10	11	11	10.5	10	11	11	10

In contrast, the corresponding maximum velocities at measurement point D1, with a distance of 77 m from borehole C2, are 37 and 105 mm/day on the 17th day after GSPG (Fig. 18).

Figure 19 shows that there is a strong correlation between the maximum velocity of deformations and the distance from the grouting borehole during GSPG according to the in situ monitoring data. This relation can be fitted by a negative exponential function with a very high coefficient of correlation ($R^2 > 0.99$), which can indicate that the velocity at some locations in the deep underground opening is very low (near zero), where it is safe, during GSPG. Workers could enter those places during GSPG. The correlations of the maximum sidewall-to-sidewall or roof-to-floor displacement velocities with the distance from the grouting borehole are expressed by Eqs. (7) and (8), respectively.

$$Y_a = 538.13 - 275.22\left(2 - \exp\left(-\frac{X}{38.87}\right) - \exp\left(-\frac{X}{38.88}\right)\right) \quad (7)$$

$$Y_b = 1.17 - 766.11\left(1 - \exp\left(-\frac{X}{40.11}\right)\right) - 1.17\left(1 - \exp\left(-\frac{X}{3.30}\right)\right) \quad (8)$$

where Y_a is the maximum displacement velocity of sidewall-to-sidewall in the deep underground opening during GSPG, Y_b is the maximum displacement velocity of roof-to-floor during GSPG, and X is the distance from the grouting borehole.
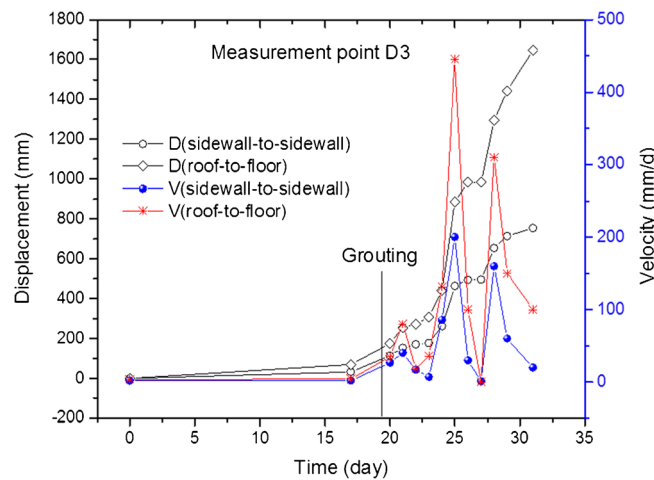
The maximum sidewall-to-sidewall and roof-to-floor displacement velocities decrease to 1.92 and 6.31 mm/day at a distance of 137 m and drop to 0.05 and 0.01 mm/day at a distance of 157 m, respectively (Fig. 19a, b). Therefore, the influence distance of GSPG on the stability of the deep underground opening is as high as 137 m but less than 157 m in the direction of the opening axis. Thus, the engineering significance of the influence of GSPG on the stability is that the underground safe distance during GSPG should be greater than 137 m.

Fig. 16 Grouting pump pressure and grouting amount of borehole C2
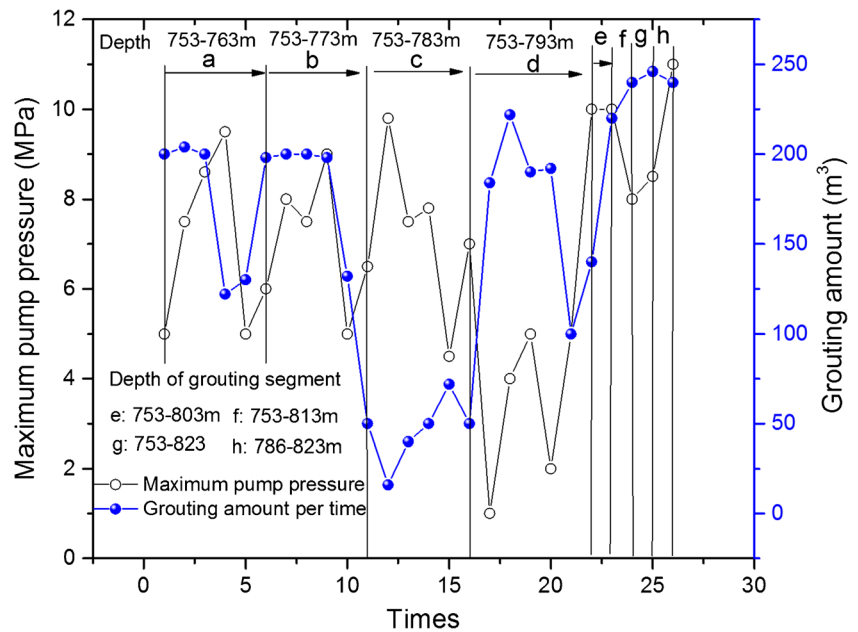
Table 9 The relationship of grouting leakage and grouting boreholes during GSPG

No.	Location	Date (month/day)	Distance relative to grouting borehole (m)		Grouting boreholes	Grouting depth when leaking (m)	Pump pressure when grouting leaking (MPa)	Amount of grouting leakage (m³)
			Horizontal distance (m)	Vertical distance (m)				
1	S68 + 180 m	1/19	51	22	C2	753–773	2	20
2	S68 + 185 m	1/25	52	12	C2	753–783	10	30
3	S68 + 185 m	1/26	52	12	C2	753–783	4.5	30
4	S68 + 188 m	1/31	53	12	C2	753–783	3.5	10
5	S68 + 180 m	2/4	50	2	C2	753–793	2.5	15
6	S68 + 180 m	2/6	54	2	B2	753–793	7	20
7	SJ52 + 261 m	2/1	40	12	B2	753–783	6	6
8	SJ52 + 84 m	3/6	72	20	A2	753–813	7	10
9	SJ52 + 84 m	3/10	72	20	C2	753–813	6	15

Fig. 17 Displacements and velocities versus time at measurement point D3

## Quality assessment of the GSPG effect

To evaluate the quality of GSPG, comprehensive methods are used, including creation of a drilling inspection borehole from the surface, UCS experiments on rock core specimens, microstructure analysis of the rock specimens, and verification of re-excavation.
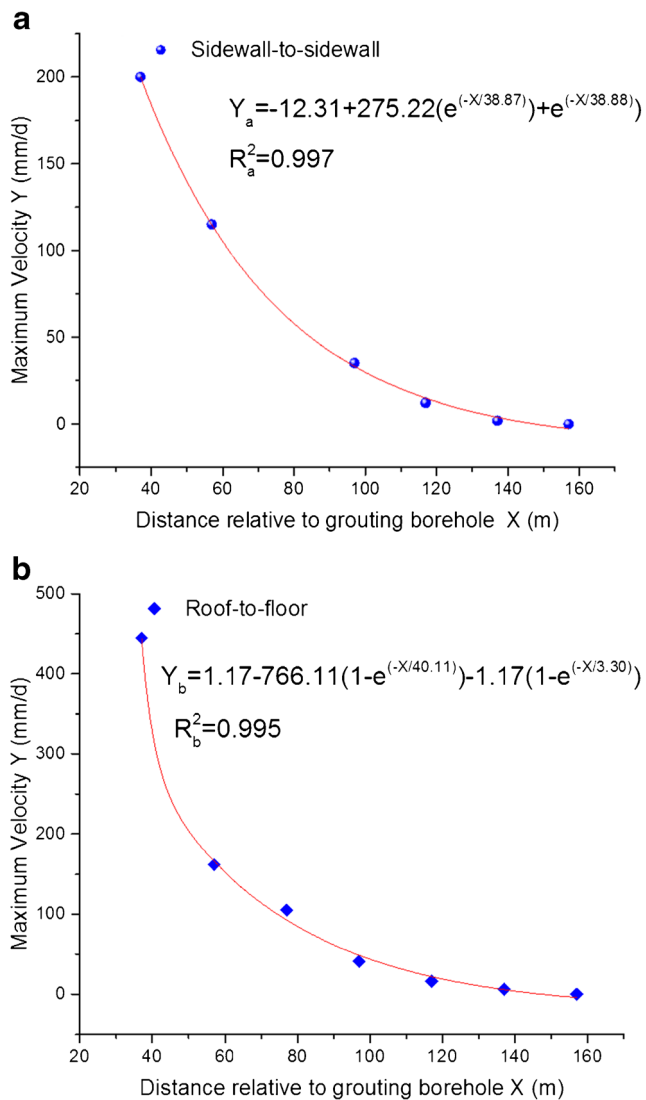
Appearance analysis of rock cores

Inspection borehole J1, used to check the GSPG effect, is drilled among the four grouting boreholes A2, C1, C2, and C3 and through the fracture zone of fault FD08 and the proposed excavation zone of the south haulage underground opening. The profiles of the borehole columnar section of inspection borehole J1 are illustrated in Fig. 20. Most of the core extraction rates are greater than 70%. The cement filling is found in rock cores of the inspection borehole.

The profiles for six representative cemented rock mass specimens are shown in Fig. 21 and Table 9. The lithology
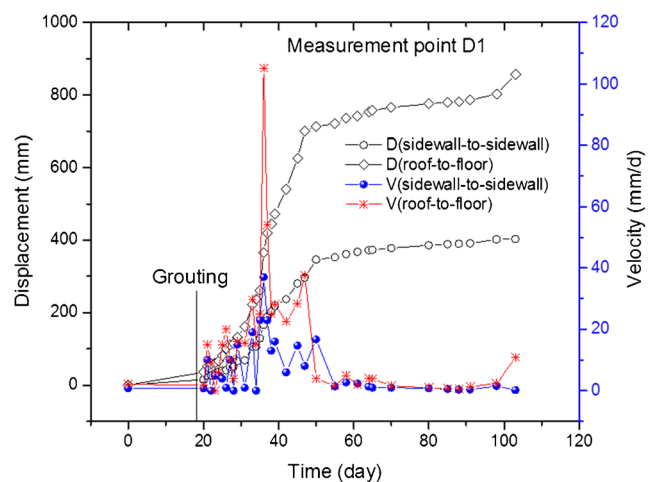
Fig. 18 Displacements and velocities versus time at measurement point D1

a

$$Y_a = -12.31 + 275.22(e^{(-X/38.87)} + e^{(-X/38.88)})$$
$$R_a^2 = 0.997$$

b

$$Y_b = 1.17 - 766.11(1 - e^{(-X/40.11)}) - 1.17(1 - e^{(-X/3.30)})$$
$$R_b^2 = 0.995$$

Fig. 19 Correlation of the maximum deformation velocity and distance from grouting borehole C2. **a** Sidewall-to-sidewall. **b** Roof-to-floor

and interior defects, such as fractures in the rock mass, are two of the main factors that impact the filling effect of cement grouting. According to appearance analysis of the cemented rock mass specimens, the cement grouting filling distribution area in the relatively good lithology and intact rock mass (specimens 1, 3, and 6) is smaller than that in the relatively poor lithology and fractured rock mass (specimens 2, 4, and 5). Generally, the cement slurry could fill the fractures, which has good cementation and reinforcement effect on the fractured rock mass. Thus, GSPG can improve the intactness of a fractured rock mass.

UCS experiment

The laboratory UCS experimental results for rock mass specimens are shown in Table 10. The UCS values of rock mass specimens reinforced by cement grouting are 4.8–48.8 MPa,

with an average of 21.3 MPa. Compared with the strength of the rock mass (below 1.6 MPa), ranked as category V before grouting, GSPG improves the strength of the fractured rock mass in the large fault zone.

Microstructure analysis of rock mass specimens reinforced by GSPG

The microstructures of rock mass specimens reinforced by cement grouting are studied using an S-3000N scanning electron microscope (SEM) made by the Hitachi Corporation (Meng et al. 2011). Comparison of the microstructures of rock mass specimens with similar lithology but different grouting appearances is conducted to analyze the variation in porosity and compactness. Specimens 1 and 5 are both sandy mudstone, but the cement grouting filling effect for specimen 5 is better than that for specimen 1 based on grouting appearance analyses. Comparing Fig. 22a with Fig. 22b, the porosity and degree of connectivity of pores for specimen 5 are lower than those for specimen 1. Hence, when the lithology of rock mass specimens is similar, the lower their porosity and connectivity is, the better the grouting effect in the rock, which means that grouting can improve the compactness and cementation strength of a rock mass. Comparing Fig. 22c and Fig. 22d, the grouting effect is similar for microstructures of medium sandstone and fine sandstone. However, the slurry much more easily penetrates into medium sandstone with larger particles than into fine sandstone. Thus, the compactness of medium sandstone is slightly better than that of fine sandstone. From the microstructures, it is obvious that network filling of slurry consolidation occurs in the rock mass, which is beneficial to reducing strata permeability and water seepage resistance.

Verification of re-excavation and field measurements after GSPG

Re-excavation reveals the cement slurry diffusion and fracture filling situation after GSPG, as shown in Fig. 23. The cement slurry fills the faults and fractures and forms the network skeleton morphology in the rock mass, which improves the mechanical properties (cohesion and internal frictional angle) of the faults and fractures and changes the stress state of the fractured rock mass from two-dimensional to three-dimensional stress. The groundwater inflow rate is less than 0.02 m³/h during re-excavation. GSPG eliminates the geohazards, including groundwater inrush, debris flow, and collapse of the large rock mass volume.

After GSPG, the united control techniques, including 8-m-long advanced borehole pre-grouting with Marithan® polyurethane chemical material (Zhang et al. 2014), U36-shaped steel sets, and 8200-mm-long cables with a diameter of 21.8 mm; 3-m-deep hole post-

Borehole column	No.	Depth (m)	Thickness (m)	Length of core (m)	Core extraction rate (%)	Rock strata	Grouting description
	1	748.00					
	2	753.20	5.20	3.60	69	Medium sandstone	Cement filling
	3	755.00	1.80	1.60	89	Sandy mudstone	Cement filling
	4	764.60	9.60	7.40	77	Mudstone	Cement filling
	5	767.20	2.60	1.60	62	Sandy mudstone	Cement filling
	6	776.20	9.00	3.60	40	Medium-fine sandstone	
	7	784.50	6.00	3.60	60	Sandy mudstone	Cement filling
	8	785.00	0.50	0.40	80	Thin coal	
	9	786.20	3.50	2.4	69	Sandy mudstone	Cement filling
	10	798.00	11.80	6.00	51	Medium sandstone	Cement filling
	11	804.5	6.50	4.00	62	Argillaceous sandstone	Cement filling
	12	808.00	3.50	3.40	97	Canbonaceous mudstone	Cement filling
	13	809.60	1.60	1.20	75	Sandy mudstone	Cement filling
	14	812.00	2.40	2.20	92	Medium-fine sandstone	Cement filling
	15	813.40	1.40	1.20	86	Coal	
	16	817.00	3.60	2.00	56	Mudstone	Cement filling

Fig. 20 Profiles of the columnar section of the inspection borehole after GSPG

grouting with fine cement for the roof and sidewalls; and 8-m-deep hole post-grouting with Marithan® for the roof, sidewalls, and floor, are conducted during re-excavation. The displacements during re-excavation are graphically presented in Fig. 24a, b. For a total of

Fig. 21 Photos of six representative cemented rock mass specimens

158 days, the sidewall-to-sidewall, roof-to-floor, and floor deformation creep rates are 0.36, 0.71, and 0.71 mm/day, respectively. The total corresponding displacements are 413, 1142, and 1139 mm, respectively. The floor displacement is much larger than that of the roof, which accounts for 99% of the roof-to-floor convergence value. Compared with the sidewall-to-sidewall (1852 mm) and roof-to-floor (3259 mm) displacements measured during the pilot excavation, the displacements decreased by 78 and 65%, respectively, during re-excavation after GSPG. The support effect of the south haulage underground opening is shown in Fig. 25. Secondary enclosed support should be further performed after floor grouting reinforcement to ensure the long-term stability of the deep underground opening through large fault zones in argillaceous rock during operation, given the creep behavior.

Re-excavation and field measurements indicate that GSPG not only achieves the effect of blocking water-bearing faults and eliminating geo-hazards but also improves the regional rock mass stability in fault zones and ensures tunneling safety.
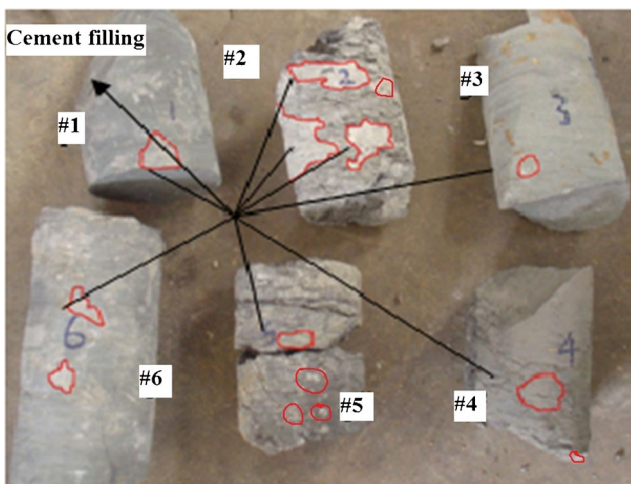
Table 10   Uniaxial compressive strength (UCS) of rock mass specimens

Rock mass specimens no.	Lithology	Depth (m)	UCS (MPa)
1	Sandy mudstone	776.2–786.2	9.5
2	Mudstone	761–764.6	4.8
3	Medium sandstone	786.2–798	48.8
4	Mudstone	801.5–804.5	7.4
5	Sandy mudstone	808–809.7	10.1
6	Sandstone	748–761	47.2
Average	/	/	21.3

Conclusions and research prospects

This study provides valuable, practical guidance for the application of GSPG reinforcement for the safe excavation of deep underground openings through large fault zones. To eliminate geohazards and ensure tunneling safety, GSPG should be first carried out to block water-bearing faults for deep underground openings with similar complex geological conditions (large fault zones) in the future. Then, collective control techniques, including underground pre-reinforcement, U-shaped steel sets, long cables, deep hole post-grouting with chemical materials, and secondary enclosed supports, can be conducted. Some conclusions and research prospects are summarized as follows.

Fig. 22 Microstructure diagrams of rock mass specimens reinforced by cement grouting. **a** Specimen 1. **b** Specimen 5. **c** Specimen 3. **d** Specimen 6
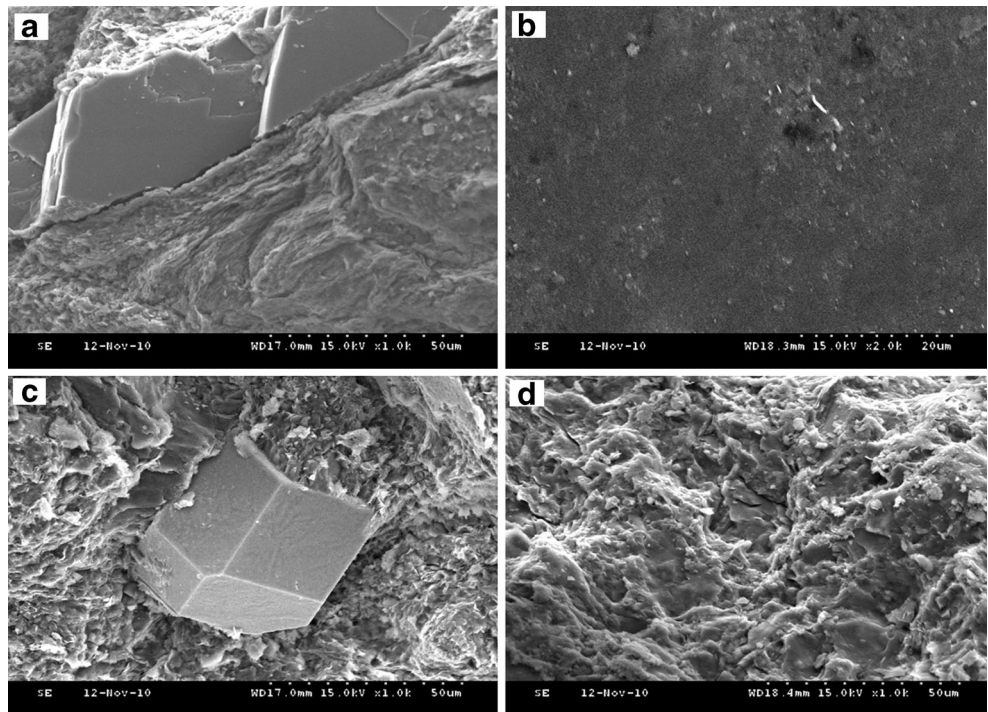
Fig. 23 Slurry diffusion and fracture filling situation that re-excavation revealed after GSPG

a

b
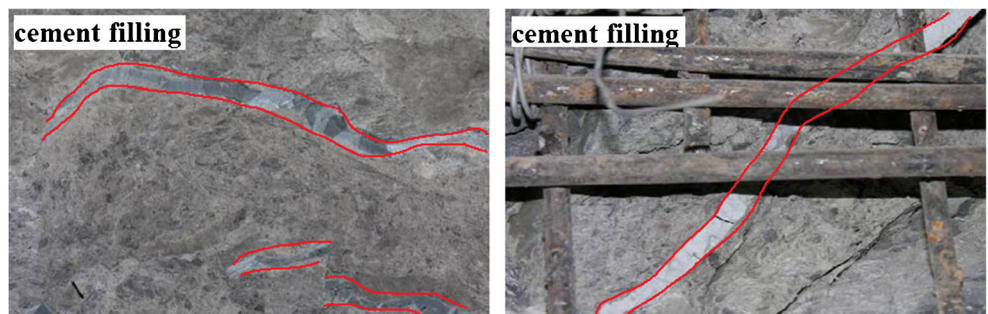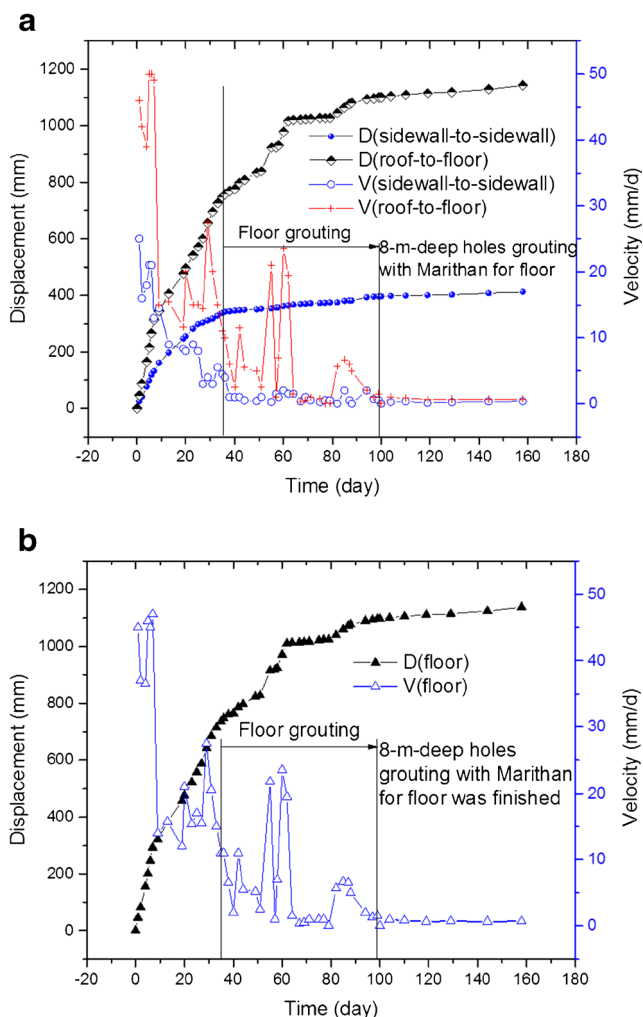
Fig. 24 Displacements versus time during re-excavation. **a** Sidewall-to-sidewall and roof-to-floor. **b** Floor

(1) The theoretical calculation of the grouting pressure using the hydraulic fracturing method provides valuable guidance for GSPG practice. Engineering practice shows that the final pump pressures for all grouting boreholes are 6–11 MPa, which are generally greater than the minimum theoretical grouting pressure (6 MPa) at a depth of approximately

Fig. 25 The completed south haulage underground opening during re-excavation

800 m. The corresponding grouting pressures at the borehole bottom are approximately 20–25 MPa, which are 2.5 times larger than the hydrostatic pressure at a depth of 800 m.

(2) A quality assessment of the grouting effect via experiment and re-excavation verification indicates that GSPG achieves the effect of blocking water-bearing faults and eliminating groundwater inrush risk, as well as improves the regional engineering rock mass stability in fault zones and ensures tunneling safety.

(3) The displacement velocity of the surrounding rock shows an obvious fluctuation response under the influence of shock loads from GSPG. GSPG significantly disturbs the stability of the deep underground opening. The impact of GSPG on the stability of an excavated 800-m-deep underground opening dramatically decreases as the distance from the grouting borehole increases. The affected distance is up to 137 m but less than 157 m along the opening axis, which indicates that the safe distance during GSPG should be greater than 137 m.

(4) The grouting slurry flow law and effective diffusion radius in a deep fractured rock mass will be investigated via numerical simulation. The mechanical analysis of the influence of shock loads from GSPG on the stress distribution around a deep underground opening will be conducted. The influence of creep and time-dependent behavior on the stability of 800-m-deep underground openings was assessed in this study only by field measurements. However, the obvious creep and time-dependent behavior of deep underground openings in argillaceous rock is a very complex issue that should be further investigated. In addition, the analytical or numerical assessment of the failure case will be presented in the future.

References

Brady BHG, Brown ET (2004) Rock mechanics for underground mining. Kluwer academic publishers, London

Brekke TL, Howard TR (1973) Functional classification of gouge materials from seams and faults in relation to stability problems in underground openings. Research report. Department of Civil Engineering, University of California, Berkeley, p 195

Buergi C, Parriaux A, Franciosi G, Rey JP (1999) Cataclastic rocks in underground structures—terminology and impact on the feasibility of projects (initial results). Eng Geol 51:225–235

Dalgıç S (2003) Tunneling in fault zones, Tuzla tunnel, Turkey. Tunn Undergr Sp Tech 18(5):453–465

Hoek E (1999) Support for very weak rock associated with faults and shear zones. In: Villaescusa E, Windor CR, Thompson AG (eds) Proceedings of rock support and reinforcement practice in mining. A.A. Balkema, Rotterdam, pp 19–31

Hao YH, Azzam R (2005) The plastic zones and displacements around underground openings in rock masses containing a fault. Tunn Undergr Space Technol 20:49–61

Huang C, Yang W, Wang Z, Feng X (2005) Field measurement study on ground perforation grouting for ultradeep soil. China J Geotech Eng 27:442–447 (**in Chinese**)

Jeon S, Kim J, Seo Y, Hong C (2004) Effect of a fault and weak plane on the stability of a tunnel in rock—a scaled model test and numerical analysis. Int J Rock Mech Min Sci 41:658–663

Lai HP, Xie YL, Yang XH (2008) Treatment effect analysis of shallow-buried crushed surrounding rocks underground unsymmetrical pressure reinforced with surface pregrouting technology in highway tunnel. China J Rock Mech Eng 27:2309–2315 **in Chinese**

Liu QS, Zhang W, Lu XL, Fu JJ (2010a) Safety monitoring and stability analysis of large-scale roadway in fault fracture zone. China J Rock Mech Eng 29:1954–1962 (**in Chinese**)

Liu QS, Gao W, Yuan L (2010b) Surrounding rock stability control theory and support technique in deep rock roadway for coal mine and application. Science Press, Beijing (**in Chinese**)

Ministry of Water Resources of the People's Republic of China (2015) Standard for engineering classification of rock mass (GB/T 50218-2014). China Planning Press, Beijing (**in Chinese**)

Meng XJ, Yao ZS, Yu G, Li J (2011) Mechanism analysis and practice of ground grouting reinforcing to geological abnormal structural belts. China Coal 37:64–66 (**in Chinese**)

Nagelhout ACG, Roest JPA (1997) Investigating fault slip in a model for an underground gas storage facility. Int J Rock Mech Min Sci 34: 97–115

Qian D (2015) Countermeasures for stability control of deep underground openings through fault zones in argillaceous rock. Dissertation, Kyushu University

Riedmüller G, Schubert W (2000) Tunnelling in fault zones-innovative approaches. In: Girard J, Liebman M, Breeds C, Doe T (eds) Pacific rocks 2000, Proc Int Congr Seattle. Balkema, Rotterdam, pp 113–124

Saito H, Date K, Narita N, Yamamoto Y, Yokota Y, Koizumi Y (2014) Pre-grouting and tunnel excavation of watertight structure section. Proceedings of 2014 ISRM International Symposium and 8th Asian Rock Mechanics Symposium, Sapporo, Japan, 1184–1189

Schubert W, Riedmüller G (1997) Influence of faults on tunnelling. Felsbau 15:483–488

Yang CL, Wang ZM (2005) Surface pre-grouting and freezing for shaft sinking in aquifer formations. Mine Water Environ 24:209–212

Yuan Y, Xue JH, Liu QS, Liu B (2011) Surrounding rock stability control theory and support technique in deep rock roadway for coal mine. J China Coal Society 36:535–543 (**in Chinese**)

Zhang DL, Fang Q, Lou HC (2014) Grouting techniques for the unfavorable geological conditions of Xiang'an subsea tunnel in China. J Rock Mech Geotech Eng 6:438–446